Remote Sensing of Environment 236 (2020) 111447

Contents lists available at ScienceDirect

Remote Sensing of Environment

journal homepage: www.elsevier.com/locate/rse

Satellite and close range analysis for the surveillance and knowledge improvement of the Nasca geoglyphs

Nicola Masini[a,*], Rosa Lasaponara[b]

[a] Institute of Science of Cultural Heritage, National Research Council of Italy(ISPC-CNR), C. da S. Loya, 85050, Tito Scalo, Potenza, Italy
[b] Institute of Methodologies for Environmental Analysis, CNR (National Research Council)-IMAA (Italy), C. da S. Loya, 85050, Tito Scalo, Potenza, Italy

ARTICLE INFO

Keywords:
Satellite multitemporal textural analysis
Principal component analysis
Unmanned aerial vehicle
Synthetic aperture radar
Integration
Nasca geoglyphs
Monitoring
Pampa de atarco

ABSTRACT:

Traditionally the history of remote sensing began during the First World War when aerial photography became a valuable reconnaissance tool. However, moving back more than a thousand years, the real pioneers of remote observation were probably the Nasca, a pre-Hispanic civilization living in southern Peru, between 100BC and 700 AD. They used 'earth observation' as a mean of cultural expression drawing the geoglyphs (known as Nasca Lines) only visible from above. These drawings were made on flat desert surface of the Pampa by removing or clearing sand or stones, to create paths for ritual functions to please the gods and create harmonious relationships between man and environment. In this paper, the Nasca geoglyphs in Pampa de Atarco, are object of remote sensing based investigations with the twofold aim to identify and characterize them as well as to analyse and monitor their fragile state of conservation, threatened mainly by vandalism and off road vehicles. The approach herein proposed includes the integration and reuse of diverse remote sensing dataset, from multispectral satellite to Unmanned Aerial Vehicle (UAV) based LSAR data and close range photogrammetry. In particular, a multidate (2002–2013) very high resolution (VHR) optical satellite dataset has been processed in the spatial and temporal domain using textural indicators, including Skewness, Principal Component Analysis (PCA), and automatic classification tools which allowed us to enhance the visibility of disturbance features and to automatically extract them. The best results in terms of enhancement and automatic extraction capability of disturbance features have been obtained by Skewness. Moreover, the reuse of UAV L SAR-based correlation map, available free of charge from NASA, provided useful information on the state of disturbance from 2013 to 2015, widening the observation time window of the VHR satellite data set from 2002 to 2013. Finally, the integrated use of satellite VHR data with UAV-based photographs and DTMs, processed using structure from motion (SfM), allowed us to characterize, identify and reconstruct the relative chronological sequence of geoglyphs thus providing new insights and opening new perspectives for archaeological studies.

1. Introduction

Earth Observation (EO) technologies have multiple potentiality and numerous applications in the cultural heritage (CH) domain ranging from the knowledge improvement to the management (Lasaponara and Masini, 2008, 2017). In the last two decades the use of EO in CH has been strongly increasing thanks to the technological improvements of the sensors ever more useful for the study of the human past and ancient landscapes for a large variety of environs including desert, tropical and Mediterranean ecosystems. In particular, the latest generation of satellite sensors opened up new frontiers and possibilities offering ever-closer and more comprehensive look at the earth's surface; providing detailed imaging even for complex and fragile archaeological heritage as geoglyphs (Hesse, 2015; Masini et al., 2016b).

As a whole, respect to the past, the archaeologists and CH decision makers are more aware of the benefits of EO technologies in terms of reduction of costs and time of archaeological investigations, and opportunities to support strategies addressed to conservation and preservation of cultural assets thanks to the:

(i) improvement in spectral and spatial resolution of sensors, evermore useful for site discovery and preventive archaeology;
(ii) availability of multiscale, multitemporal and multi sensor data useful to investigate changes due to human activity in areas of cultural interest and monitoring risk in archaeological sites.

Moreover, today these technologies are available at different costs, for different purposes and needs, and even with small budgets it is

* Corresponding author.
E-mail addresses: nicola.masini@cnr.it (N. Masini), rosa.lasaponara@imaa.cnr.it (R. Lasaponara).

https://doi.org/10.1016/j.rse.2019.111447
Received 15 May 2019; Received in revised form 22 July 2019; Accepted 23 September 2019

possible to implement very effective solutions, but, they pose several issues related to the processing, integration, analysis and interpretation of data (Opitz and Herrmann, 2018). These issues are the challenges to face for transforming data into useful and reliable information and, therefore, they must be tackled by the scientific community in order to ensure an effective and reliable applicability of EO, as also expected in the Copernicus Programme initiatives (Casu et al., 2017). These require efforts also addressed to bridge EO technologies and archaeological communities to overcome the current limitations. In this context, significant contributions can be also achieved via case study demonstration useful to support the development, application, assessment and improvement of reliable automatic data processing approaches and integrated methodologies of data analysis and interpretation. (Luo et al., 2019).

In this paper, we focus on the analyses of Multitemporal/Multisensor data, collected from satellite, UAV and ground, to obtain meaningful and detailed information about the changes that over time have affected the geoglyphs made by Nasca civilization in Southern Peru. They are only visible from above and are considered one of the most fragile and vulnerable world heritage sites (https://whc.unesco.org/en/list/700). This is because they were made: (i) removing and pulling the gravel inwards to the drawn lines, to obtain the figures in slight relief or (ii) through the removal of the gravel to obtain solid figures by the resulting contrast with its surroundings (Eitel, 2005); and, moreover, (iii) they sparsely spread up over huge areas with easy access, which make their destruction almost effortless and their protection very challenging (Masini et al., 2016b). These characteristics highlight the challenges and urgent needs related to their protection and preservation issues being that Nasca geoglyphs provide a unique and invaluable source of information about Nasca civilization that flourished in the distant past. For these reasons, specific surveillance and monitoring strategies must be adopted to safeguard them.

The methodology herein devised is based on the use of heterogeneous information from multiple EO data sources *ad hoc* processed to improve knowledge and set up monitoring methodologies of geoglyphs and their surrounding landscape. Knowledge improvement is a mandatory step for the preservation especially for the specific characteristics of geoglyphs and Nasca Lines considering the difficulty in recognizing and detecting them in particular for those located in Pampa de Atarco. In fact, the specific drawing techniques (see section 2.3) of these geoglyphs make them very difficult to see not only from on ground, but also from above (from airplane, drone and satellite). For this reason, Pampa de Atarco (see section 2) has been herein selected as test site, to develop a suitable methodology, based on remote sensing (the only tool applicable for geoglyphs!), to enhance the visibility of geoglyphs and to capture and extract changes that adversely affecting them.

Our effort is a contribution to the definition of the best practices for the production of critical information necessary for improving the knowledge and set up a reliable and systematic monitoring. This is pursued by: (i) exploiting historical and updated data available from remote sensing technologies from satellite, manned and unmanned aerial vehicles (UAVs), (ii) defining *ad hoc* data processing to enhance, detect and characterize geoglyphs features, (iii) using key statistical indicators to capture and quantitatively evaluate the impact of changes, (iv) the validation of the outputs from satellite data by using close range data. In particular, the use of statistical analysis (PCA and Skewness) along with unsupervised classification allowed us not only to identify and delimiting disturbance, but also to extract in automatic way suitable information useful to face the ongoing threats and facilitate the operational activities and preservation strategies.

The methodology herein proposed can be promptly re-applied to other cultural heritage sites with particular reference to those characterized by geoglyphs which were a cultural phenomenon common to several civilizations in different historical periods and geographical regions. In particular, the drawing of figures only visible from above, was very common in Americas, see, for example, the serpent-mound in Ohio, the ornithomorphic figures in Wisconsin (Orefici, 2009), the geoglyphs in the Atacama desert of Chile (Briones, 2006), channels and embankments depicting geometric figures in the Acre state (Brazil) (Saunaluoma and Schaan, 2012), and, finally, the ring ditches in the Bolivian Amazon (Erickson, 2010). In Peru, the geoglyphs were drawn usually on the desert coast, where the sandy loam soil, covered by alluvium, was more suitable for their conservation, see, for example, the Condor de Oyotún and the anthropomorphic figure in Pampa de Caña Cruz in the Lambayeque region (Alva and Meneses Alva, 1984), the geoglyphs of Canto Grande, near Lima (Roselló et al., 1985), and, of course, the well known Lines and Geoglyphs of Nasca and Palpa, listed in World Heritage since 1994 (https://whc.unesco.org/en/list/700).

2. Study area and data set

2.1. The geoglyphs of Nasca: technical aspects and cultural meaning

The Nasca Lines are one of the most impressive cultural heritages in the world, dated from 200BC to 600 AD and created by Paracas and Nasca civilizations considered among the richest, most refined, and original cultures of the pre-Hispanic Andean world (Silverman, 1990; Masini et al., 2016). These geoglyphs were obtained using three different engraving techniques by: (i) removal of gravels and sand to evidence the underlay lighter dust, (ii) adding dark colour pebbles and sand grains along the lines, (iii) creating slight micro-relief by scraping sand and gravels and adding some darker gravel along the edges of the figures (Eitel, 2005; Masini et al., 2016a).

The impressive geoglyphs shapes, huge sizes (lines longer more than 1 km and biomorphic figures reaching up to 300 m; see Fig. 1bcd), and, functions have attracted an extraordinary scientific interest. In the last century, diverse assumptions and numerous theories have been postulated among them the main is the astronomical one, which considers the Nasca lines as a “great book” of astronomy with the function of a calendar (Kosok and Reiche, 1949; Aveni, 1986). The latest theories are based on the spatial/cultural/religious relationship between (i) the mountains and sacred places (Reinhardt, 1988); or (ii) between geoglyphs and settlements (Reindel and Wagner, 2009), and Cahuachi ceremonial center (Silvermann, 1990; Orefici, 2009; Masini et al., 2016a). According to these latest theories, the geoglyphs were sacred spaces used as “venues” for civic ceremonial activities and pilgrimage paths.

As a whole, the phenomenon of the geoglyphs has its origin in a profound religious and cultural substratum, strongly influenced by the extreme conditions of the climate and environment where the Nasca used to live. Therefore, the geoglyphs were a cultural expression of the need of adaption, a request of help to the gods, an attempt to create harmonious relationships between man and environment, earth and sky made by ceremonial activities performed in the geoglyphs sacred space (Masini et al., 2016a,Masini et al., 2016). Geoglyphs were made to please and to be seen by Gods, therefore, only visible from above.

2.2. Protection issues

Due to their specific characteristics, geoglyphs are very fragile because they can be severely damaged or completely destroyed simply stepping on them. Therefore, the protection of this vast area is a mandatory issue to reduce threats mainly due to tourism and vandalism (UNESCO, 1994). For these reasons, Peruvian Law No. 24047/19, put the National Institute for Culture in charge to protect these geoglyphs, the access was forbidden and the planning for urban and rural development limited. But, despite this, unfortunately, over the years, numerous disturbances have left indelible traces on the landscape as, for example, tracks made by vehicles or feet, including those linked to the Dakar auto rallies of 2012 and 2013, and other damage (Kozak, 2014).

In 1993, the Lines and geoglyphs of the Pampas of Nasca spreading

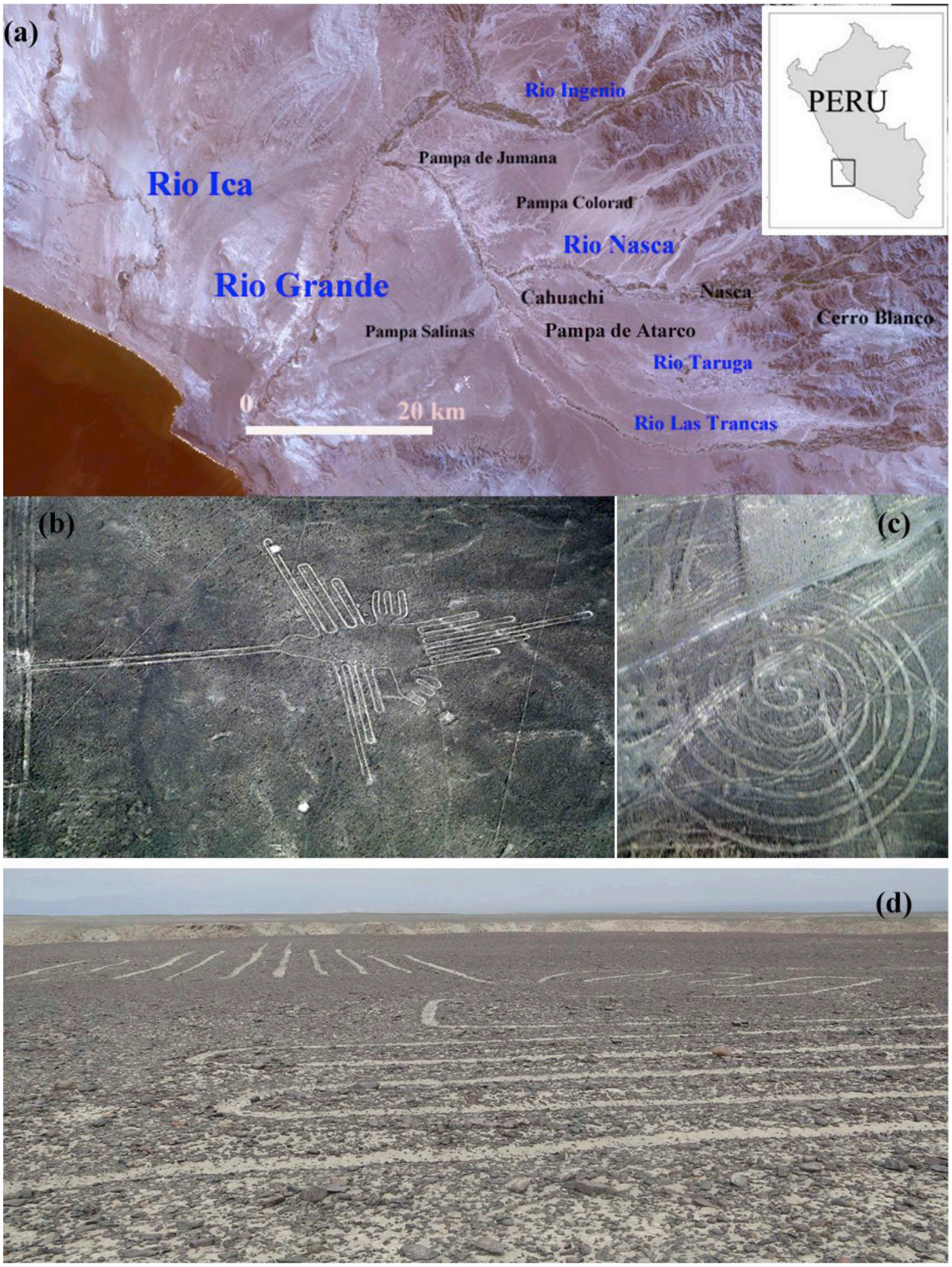

Fig. 1. . (a) Landsat TM acquired in 2008 of Rio Grande drainage basin, in Southern Peru, including the Pampa de Jumana characterized by the most famous geoglyphs (among which those showed in Fig. 1b and c), Pampa de Atarco which is the area under investigation of this paper, the Ceremonial center of Cahuachi, and the tributaries of the river, among which Rio Nasca. (b–c) Aerial images (© Nicola Masini) of the famous hummingbird and a spyraliform motif located in Pampa de Jumana. (d) The hummingbird seen from the ground (courtesy by Giuseppe Orefici).

over more than 700 square km2 along low foothills and desert terrain were declared Archaeological Reserve Area and later on in 1994 inscribed on the World Heritage List. According to the 2013 UNESCO report, the factors affecting the geoglyphs are: i) illegal farming and mining activities; ii) vehicular tracks; iii) flooding; iv) lack of systematic monitoring; v) insufficient air-traffic security measures; vi) lack of a management plan.

On the January 16, 2015, a Resolution of Peruvian Ministry of Culture (No. 019-2015-MC) approved the “Management System for Cultural Heritage Nasca and Palpa Territory” plan that covered not only

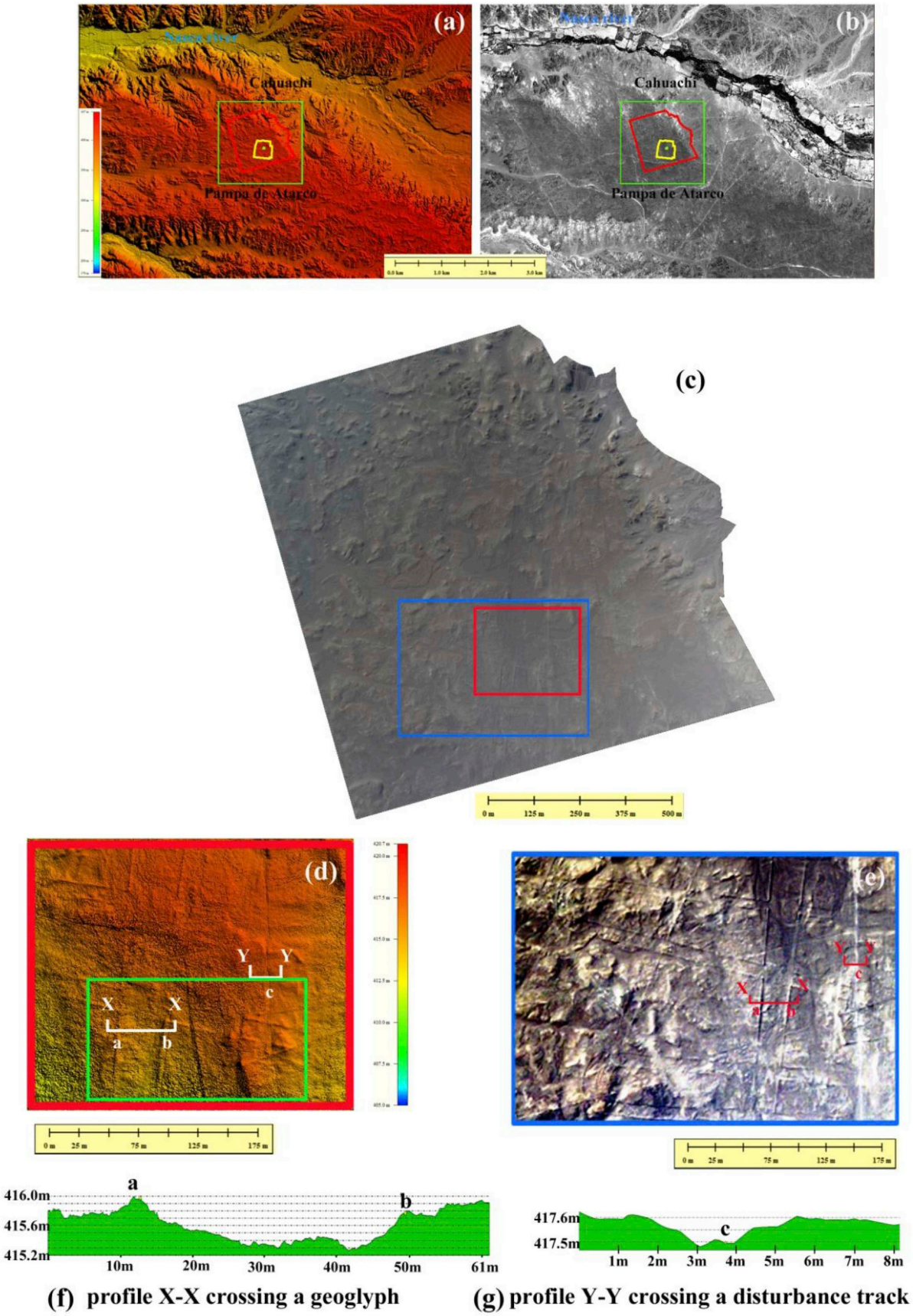

Fig. 2. (a), (b) Satellite based DEM and orthophoto of Pampa de Atarco geoglyphs, Nasca River and Cahuachi with identification of the area under investigation, indicated with green box. Red and yellow polygons indicate the areas of aerial and drone surveys, respectively. (c) Orthophoto obtained processing aerial images by SfM. (d) Detail of aerial orthophoto whose location is indicated with blue box in Fig. 2d. (e) Detail of UAV-based DEM whose location is indicated with red box in Fig. 3c. (f–g) Profiles X-X is related to a trapezoidal geoglyph, whereas profile Y–Y is related to a disturbance track (see also Fig. 2d); a and b, in Fig. 2f, refer to the edges of the trapezoidal geoglyph. c refers to the track (see also Fig. 2d and e). In Fig. 2d green box indicates the area that will be showed in Fig. 10.

the UNESCO mapped area but also a larger territory (over 5627 km2) which also included the geoglyphs of Pampa de Atarco object of analysis in this paper.

2.3. Study area: pampa de atarco geoglyphs

Pampa de Atarco, located at 2–4 km south of the pyramids of the ceremonial center of Cahuachi, at 5–7 km south of the Nasca river (see Fig. 1a, 2a-c), fits into the hollow of the *Rio Grande de Nasca* river systems, tributaries of the Río Grande, dating from the Tertiary and Quaternary periods. It lies on an important impermeable base made up of metamorphic, sedimentary, and intrusive rocks (Delle Rose, 2016; Orefici and Lancho Rojas, 2016; Schreiber& Lancho Rojas, 2009).

Previous studies (Masini et al., 2016a) highlighted a spatial and functional relationship between the geoglyphs of Atarco and the temples of Cahuachi. Both Geoglyphs and temples were sacred places used by the Nasca for religious ceremonies and other liturgical forms of religion; hence the cultural importance of the geoglyphs of Atarco.

As regards the morphological characteristics, the presence of geometric figures is prevailing as straight lines, trapezoidal, rectangular, spyraliform, and meandering motifs. From the execution point of view, all the three different techniques, already described in 2.1, are present. In Pampa de Atarco, the use of sand grain, pebbles and gravel of small dimension (gravel size ranging from 8 to 20 mm, pebble size from 70 to 120 mm; see Fig. 3b) make the geoglyphs very difficult to see on ground (Fig. 3a) and, in not optimal illumination conditions even from air craft (Fig. 3c) or drone. This makes necessary the use of diverse remote sensing dataset and processing techniques aimed at enhancing edges and texture of the geoglyphs.

2.4. State of the art of remote sensing of Nasca geoglyphs

Despite the great interest in studying geoglyphs using observation tools from above, up to now, a few attempts have been only made to evaluate the performance of EO for the monitoring, protection, and preservation of geoglyphs of Nasca, and Palpa. In the last decade, a few but significant studies have been conducted using SAR earth observation technologies.

Ruescas et al. (2010) used the radar coherence to assess changes of the Nasca Lines from 1997 to 2004. In particular, they used two pairs of satellite SAR data: the first acquired by ERS-2 SAR from 1997 and 1999; the second one by ENVISAT-ASAR from 2003 and 2004. Several different decorrelation factors contributing to a loss of coherency in a radar pair can be distinguished, and these include the temporal change in the ground properties and nature between the two satellite passes (Ruescas et al., 2010).

Chapman et al., (2015) evaluated the potential of NASA/JPL UAV SAR for examining the condition of the Nasca geoglyphs. In particular, L-band data were collected almost exactly two years apart, on 19 March 2013 and on 21 March 2015. In particular, they used the repeat-pass interferometric pair to detect disturbance affecting the Nasca lines, including erosion phenomena. Following Chapman et al., 2015, the same author group (Comer et al., 2017) integrated the L-band from UAV with Sentinel-1 C-band to detect landscape disturbance threatening Nasca and Palpa Lines. Cigna and Tapete (2018) used COSMO-SkyMed InSAR for tracking some human-induced disturbance close the famous hummingbird.

As regards optical data, Lambers (2006) used aerial photogrammetry for the documentation and morphological characterization of the Palpa geoglyphs. Hesse (2015) investigated a Landsat TM time series (2009–2013) to identify disturbances affecting the Lines. He pointed out that the most extensive surface disturbances occurred between 06 January 2012 and 22 January 2012, due to the intense off-road vehicle linked to 2012 Dakar rally which passed close to the area. Finally, very high resolution optical satellite imagery have been used by Masini et al. (2016a,b) for mapping the Ceremonial centre of Cahuachi and the geoglyphs of Pampa de Atarco, with the twofold aim to provide new information on the function of these geoglyphs and to map disturbance caused by off-road vehicles and urban sprawl. The approach was simply based on the visual reconnaissance of both geoglyphs and disturbances affecting them.

In this paper, we focused on the challenging issue of setting up a multiscale and multisensor methodological approach (i) to facilitate the visual identification of geoglyphs of Atarco, which are much more subtle and difficult to be recognized (see Fig. 3) compared to those of Palpa and Nasca, and (ii) to detect changes linked to anthropic disturbances, evaluating the opportunities to extract them in an automatic way.

3. Methodology

The approach herein proposed is based on the identification of key statistical indicators useful (i) to enhance and characterize geoglyphs, and (ii) to automatically detect and extract changes linked to disturbance. To this aim, we adopted an integrated approach, based on diverse remote sensing technologies and analyses, including close range RS data. On the basis of the availability of data, we used a multitemporal (2002, 2005, 2011 and 2013) optical VHR data set and UAV L-band SAR survey acquired in 2013 and 2015 and processed by NASA. Finally, aerial and drone surveys were conducted in September 2015 in a significant subset of the investigated area. The analyses were conducted using the optical satellite data listed in Table 1.

After the preprocessing (calibration, atmospheric correction, orthorectification), the satellite optical VHR images were processed using multi-temporal Principal Component Analysis (PCA) and texture to enhance, speed, and improve the identification of both geoglyphs and disturbances. In particular, the information on the texture is herein performed in both spatial and temporal domains. Mathematical procedures used to extract texture features, can be categorized into three general approaches: (i) statistical analysis (as for example PCA), (ii) model-based methods, and (iii) signal processing methods, including Fourier transforms, convolution filters, co-occurrence matrix, spatial autocorrelation, fractals, etc. In this paper, the investigations were performed as follow:

(a) Four VHR satellite optical images were processed using multitemporal analysis based on: (i) PCA (ii) textural indicators, including Skewness, and (iii) unsupervised classification of PCs and Skewness;
(b) Re-use of two date acquisitions of L-SAR UAV as processed by NASA to obtain the interferometric correlation (Chapman et al., 2015).
(c) Processing of RGB images taken from air flight and drone using Structure from Motion (SfM), to obtain orthophotos, digital elevation models (DEMs), and further enhancement of DEMS-micro-topography using Simple Local Relief Model (SLRM) and Sky View Factor (SVF);

The processing of VHR satellite data was only based on the panchromatic scenes because, according to previous investigations of the same author group (Masini et al., 2016a), in this desert area, the multispectral channels do not provide significant additional information compared to panchromatic and, therefore, we preferred to exploit the higher spatial resolution.

3.1. Processing the optical very high resolution (VHR) multi-date satellite imagery

3.1.1. Principal components analysis and skewness

The need to identify and characterize changes mainly due to human induced disturbance (from footpaths to vehicle tracks) makes necessary to perform multitemporal analyses. To this aim, PCA and textural analyses, based on Skewness, have been used.

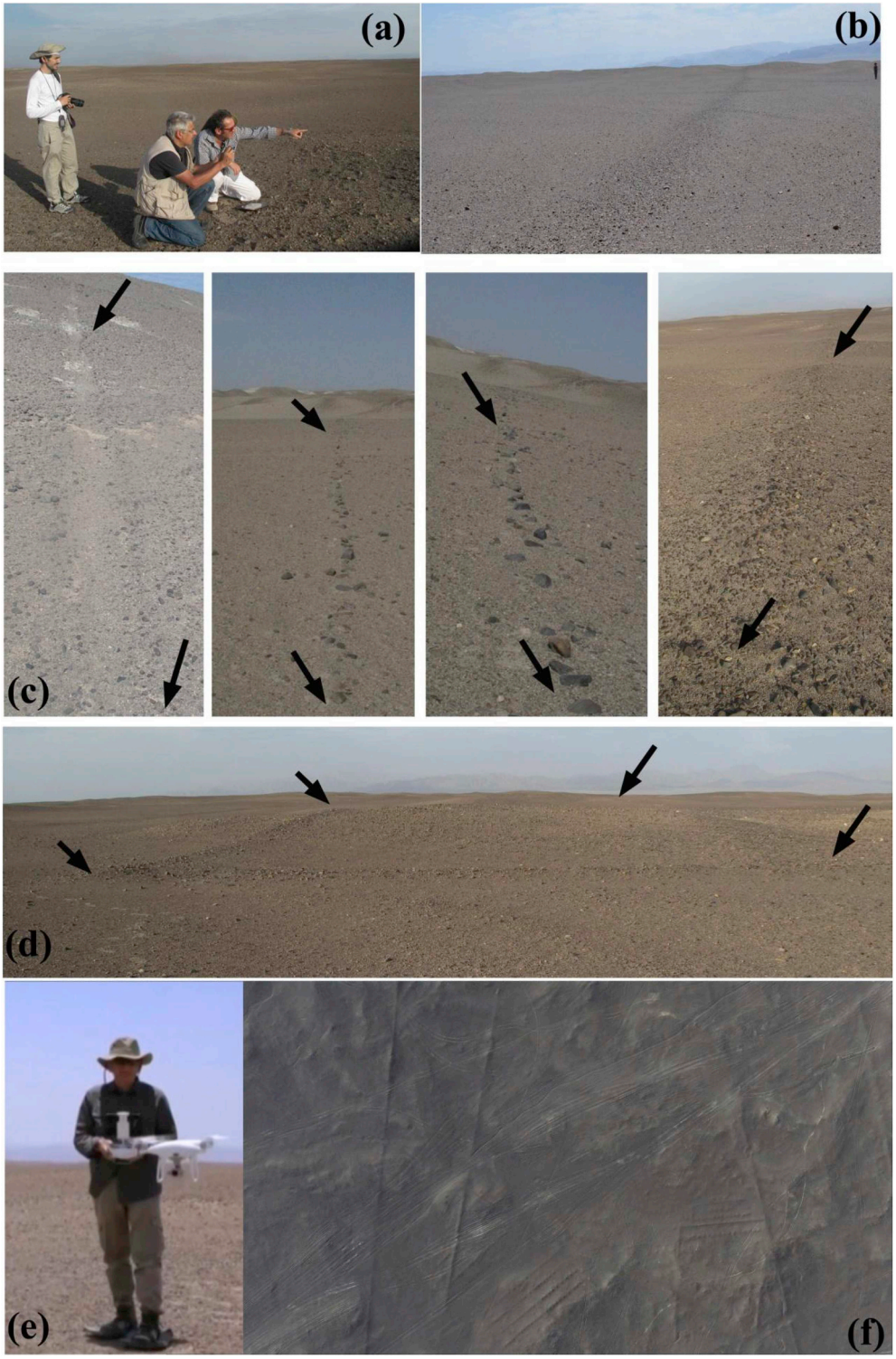

Fig. 3. All ground operations (2a), including drone driving (2e), have been carried out with all possible precautions such as the use of particular shoes, GPS with satellite images and maps in order to avoid to damage geoglyphs stepping on them. These images show how fragile are the geoglyphs and how difficult to identify them on ground (2b, 2c, 2d) and by drone (3f). The ground images (2a-2e) are by Rosa Lasaponara; The oblique aerial image taken from UAV is by Antonio Pecci.

The PCA (see, for example, Richards and Jia, 2006; Neeti and Eastman, 2014) is a mathematical transformation that is useful and used to remove redundancy in a given multi-band (multispectral or multitemporal) data set through the creation of a new image data set with fewer uncorrelated components. This is obtained by translating and/or rotating the axes of the original feature space, using a linear transformation to decorrelate multivariate data and represent them in a new component space without correlation.

To do this, the process computes the covariance (or variance) matrix (S) among all input time series, the eigenvalues, eigenvectors and loadings using the formulas shown in the Appendix.

The most common application of PCA is based on the use of

Table 1
Satellite optical VHR data set: acquisition time, satellite sensors, ground sample distance (GSD).

Acquisition date	Satellite sensor	Panchromatic GSD (m)	Multispectral GSD (m)	Time	Other
16.09.2002	QuickBird-2	0.619	2.48	15:17	
25.03.2005	QuickBird-2	0.634	2.54	15:29	
28.02.2011	Stereo GeoEye-1 *	0.50	2.00	15:30	DEM
13.03.2013	Pléiades 1B	0.50	2.00	15:20	

covariance matrix, even if both variance and covariance measure the "spread" of a dataset around the mean. A series of new image layers (eigenvectors generally called eigenchannels or components) are obtained from the eigenvalues of the covariance matrix.

PCA allows us to highlight the area (pixels in this case) affected by changes, due to the low correlation associated (in multi-temporal dataset) to the pixels that change substantially. The major portion of the variance in a multi-temporal image data set is associated with non variable surface characteristics and will be mainly in the first component; whereas, pixels/areas of localized change will be enhanced in later components. To correctly interpret the results obtained from the PCA additional information (as loadings, ground survey, etc.) are required being that the eigenvectors are extracted from the series itself and, therefore, they cannot have a general and universal meaning.

Along with PCA, we also considered the Skewness (Balakrishnan and Scarpa (2012), applied in the temporal domain, in order to detect changes. Skewness measures the degree of distortion from the symmetrical normal distribution informing on how much and in which direction, the values deviate from the mean, median and mode. The Skewness can be determined by how these quantities are related to each other, and for this purpose there are several formulations that are also available in image processing tools (https://www.itl.nist.gov/div898/handbook/eda/section3/eda35b.htm). The most common skewness measurement is Fisher-Pearson (or Pearson median skewness) expressed by the formulas reported in the Appendix.

3.1.2. Unsupervised classification and segmentation

To automatically extract changes, outputs from PCA and Skewness were further processed using unsupervised classification selected because: (i) it is an automatic process, (ii) classes do not have to be defined a priori; and, moreover, (iii) unknown features/classes may be identified and categorized.

Unsupervised classifications can be performed using different approaches/algorithms, as: (i) K-means clustering, and (ii) ISODATA (Iterative Self-Organizing Data Analysis Technique) (Ball and Hall, 1965). In this study, ISODATA was applied because more flexible compared to k-means which a priori assumes the number of clusters.

The classification is followed by a segmentation step to reduce the complexity of the classification outputs and facilitate the image interpretation. The segmentation process requires the following three parameters: (i) Colour, (ii) Scale, and (iii) Form (Shape).

The first parameter balances the homogeneity of segment colour and shape: value "one" will result in very fractal segments (with a low standard deviation), whereas a zero value in very compact segments (with higher colour heterogeneity).

The scale parameter is an abstract value without any direct correlation with the object size, and it depends, rather, on the heterogeneity of the data, performed setting: i) the minimum number of pixels for building a segment (in our case set equal to 50; ii) the number neighbouring pixels which determines the separability/connectivity of the segments (set equal to 4).

Finally, the form parameter controls the form features balancing the criteria for border smoothness and object compactness.

3.1.3. Spatial texture analysis

Texture analyses have been also performed in the spatial domain to enhance edges of geoglyphs features and, therefore, to facilitate their identification from above. Texture is not an absolute parameter, but, it is function of spatial and radiometric resolution and according to the given scale can be fine, rough, rippled, smooth, and irregular (Irons and Petersen, 1981). In this paper, texture analysis has been performed using co-occurrence measures and the relative outputs are based on several indicators such as mean, variance, dissimilarity, entropy, etc (see equations (7) to 12) shown in the Appendix) to quantitatively evaluate the textural parameters. The texture categories herein used are based on distinguishing features obtained from the Mean and Standard Deviation which are the local mean and standard deviation values obtained for the selected size of the processing window, as well as from the Variance, Correlation, Contrast, Dissimilarity, Homogeneity, and Entropy computed as shown in the Appendix. These indicators are all computed on a single scene and then compared with the output obtained over time from all the available multi-temporal data sets (acquired on 2002, 2005, 2011, 2013; see Table 1). Outputs form texture analysis have been classified using the approach describes in section 3.1.2.

3.2. Reuse of UAV SAR interferometric coherence

The UAVSAR data were processed by NASA (Chapman et al., 2015; Comer et al., 2017) and available online free of charge (https://uavsar.jpl.nasa.gov/cgi-bin/data.pl). Among the products, we used the correlation image computed from the SLC data, to identify the changes occurred between the two years of acquisition 2013–2015 in order to integrate those mapped from the VHR satellite between 2002 and 2013.

The correlation was computed as follows using formula:

$$\hat{\gamma} = \frac{\sum_{n=1}^{N} s_{1n} \cdot s_{2n}^{*} \cdot ((1 + SNR^{-1}))}{\sqrt{\sum_{n=1}^{N} |s_{1n}|^2 \cdot \sum_{n=1}^{N} |s_2|^2}} \quad [13]$$

where.

N is the number of pixels in the coherence window calculated,
S_{1n} and S_{2n} indicate the complex value of master and slave image, respectively,
indicates conjugate operator, and
SNR is the signal-to-noise ratio

The correlation γ can vary between 0 (complete decorrelation or, equivalently, no correlation between the two images) and 1 (no decorrelation or, equivalently, complete correlation between the images). The need to normalize γ by the SNR is due to the fact that some areas, shadowed by topographic features, may have a correlation greater than 1.

Some authors have reported promising results from investigations on the relationship between InSAR coherence (correlation) and changes in superficial cover and/or other characteristics (Chen et al., 2016). It is expected that the use of interferometric may enhance changes, thus improving the identification and characterization of archaeological remains.

Table 2
Data of Manned and unmanned aerial acquisition.

Acquisition type	Acquisition date	Time	N. images	Camera	DEM GSD (cm)	Orthophoto GSD (cm)
Manned aerial acquisition	**01.09.2015**	07:15	15	Canon EOS 6D: Digital single-lens reflex camera featuring a full-frame (approx. 35.8 × 23.99 mm) CMOS sensor with approx. 20.2 effective megapixels	31.70	15.90
Unmanned aerial acquisition by Dji Phantom Vision 2	**04.09.2015**	06:10	210	Camera with the following characteristics resolution 14 megapixels, FOV 120°/110°/85°, Sensor size 1/2.3″	5	2.5

3.3. Manned and unmanned aerial image acquisition and processing

Close range acquisitions were performed in 2015 taking photographs using a RGB camera from an ultra light aircraft (see Table 2). The aim was to identify subtle geoglyph features and characterize the superposition of drawings in order to understand the relative sequence by the interpretation of oblique photos, DEMs and orthophotos.

The surveyed area was the center of the meandering figure. Some detailed images were acquired using a drone Dji Phantom Vision 2, mounting a 14 megapixels RGB camera.

Both manned and unmanned aerial images have been processed using SfM algorithm in Agisoft Photoscan software ver. 1.4.

To appreciate the microtopography with centrimetric detail for the interpretation of geoglyphs and disturbance features, the DEMs obtained from both manned and unmanned images were enhanced using a number of visualization techniques, including hill shading, simple local relief model (SLRM) and Sky View Factor (SVF).

From the computational point of view, SLRM (Hesse, 2010) approach is based on the: (i) smoothing of DEM made applying low pass filter, (ii) its subtraction to the initial DEM, (iii) calculation of the zero meter contours from the difference model to obtain break lines, as well as the intersection of the break lines with the DEM. SLRM computation is based on the use of a kernel within computing the statistical parameters and, obviously, the results will strongly depend on the kernel selection.

SVF (Zakšek et al., 2011) quantifies 'the portion of the sky visible from a certain point' within a certain radius, in other words large SVF denotes a large portion of the sky visible and the size of the observed area (defined by the chosen radius) impacts on the result. Small radius is required (e.g., 10–15 m) to highlight subtle and small-scale microrelief as expected in the geoglyph area. In particular, SVF delineates mainly concave features and maintain the slope well visible also preserving the perception of the general topography.

4. Results and discussion

A visual inspection of the multitemporal satellite images clearly put in evidence that these data, without a specific data processing, do not provide the details necessary to (i) analyse the morphological features of the geoglyphs and (ii) identify changes affecting them (with particular reference to anthropic disturbances). As an example, Fig. 4(a–d) shows a detail of a meandering geoglyph, thought to be linked to ceremonial activities performed by the Nasca people, walking in procession, singing and praying on the ground drawing (Masini et al., 2016a; Orefici, 2009). This scene, from now on, will be assumed as reference for the following figures. It is characterized by the presence of geoglyphs shaped as lines (in particular a trapezoid) and curvilinear elements, obtained by the removal and addition of stone material to create micro-relief (see Fig. 2 in section 2.3 and also details from UAV derived DEM in Fig. 3d–f).

As regards the disturbance features, only the big tracks caused by off-road vehicles are visible, as indicated in Fig. 4 by coloured arrows and letters d1, d2, d3, d4, and d5. They have a wide that ranges from 4 to 16 m. As a whole, we can argue that the visual comparison of the panchromatic scenes shows the biggest changes and a different frequentation of the tracks, in one case continuous (see d2 in Fig. 4), in other cases more sporadic.

4.1. Multitemporal analysis for disturbance identification and automatic extraction

Some statistical computations (using ENVI tools) have been performed to enhance geoglyphs, and changes affecting them, and to overcome the subjectivity of the visual comparative analyses. In particular, three strategies have been adopted to extract information and translate data into useful, operational, and meaningful information. In

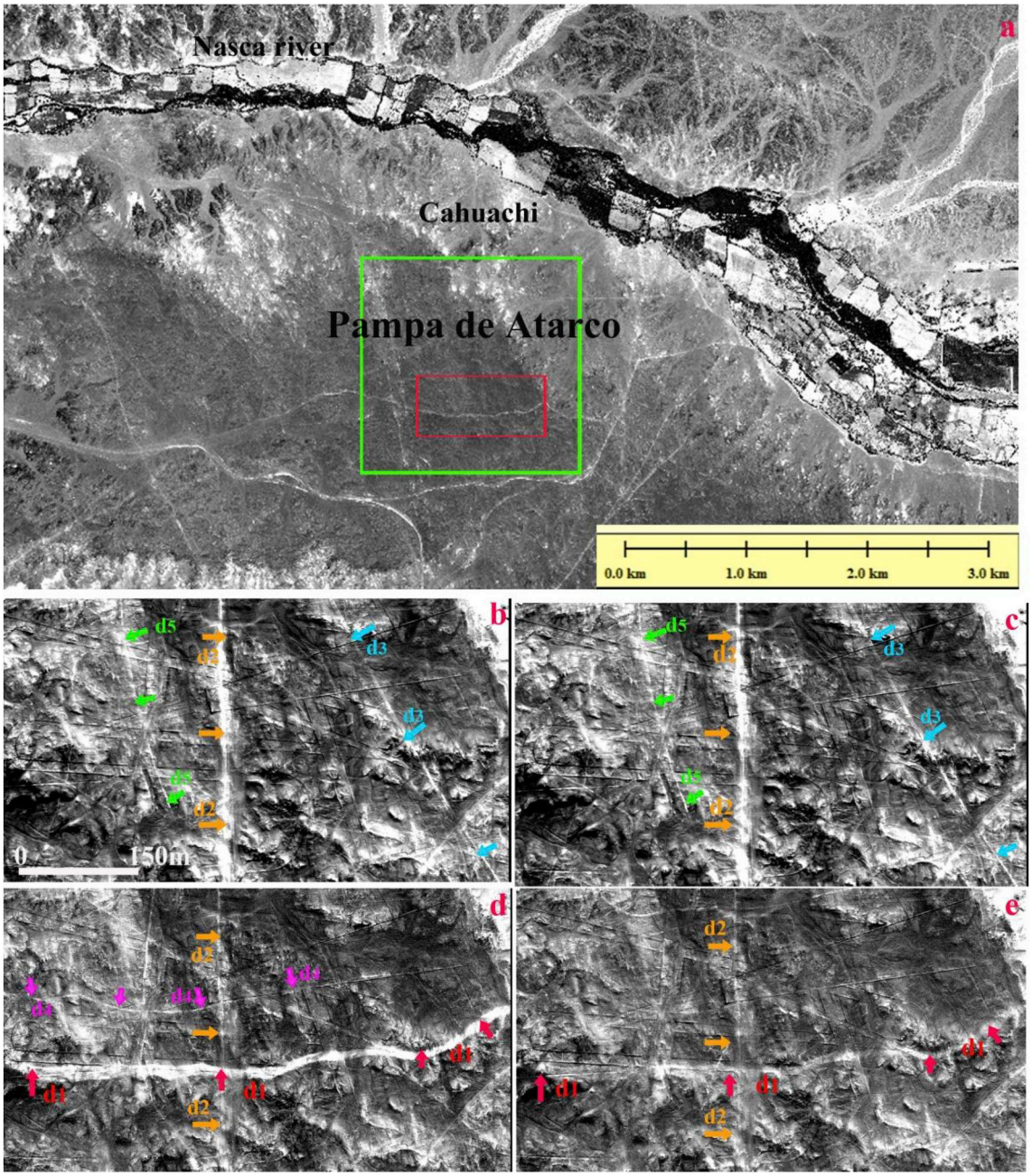

Fig. 4. (a) 2011 GeoEye panchromatic image. The green box indicates the whole area under investigation. The red box is the subset herein discussed and showed as multitemporal date set in b-e. In particular, (b) 2002, (c) 2005, (d) 2011, (e) 2013. The coloured arrows and the letters d1-d5 denote disturbance tracks caused by off-road vehicles. (For interpretation of the references to colour in this figure legend, the reader is referred to the Web version of this article.)

particular, we used:

i) PCA and Skewness to identify and characterize disturbance features from 2002 to 2013
ii) Unsupervised classification and segmentation to automatically identify and map changes
iii) SAR correlation map for estimating the changes occurred from 2013 to 2015

Outputs from PCA are in Fig. 5 which shows the four principal components as obtained from the multitemporal panchromatic satellite dataset.

The first component (PC1) accounts for the majority of the total dataset variance exhibiting strong correlation values among the four input scenes.

As expected, being that PC1 is an integral/average value, and considered that geoglyphs are quite stable over time (for more than one thousand years ..!), it enhances geoglyphs and potential permanent disturbance, as in the case of the central black track (indicated with orange arrows and letter d2) caused by off-road vehicle, south-north oriented, and visible since 2002 (see Fig. 4). It has a wide that ranges from 3 to 5 m and is present in all the scenes (from 2002 to 2013, see Fig. 4a–d) thus indicating that it has been used continuously. On the basis of the previous consideration, we can point out that PC1 well enhances the geoglyph edges and maintains the traces of disturbances permanently present in the whole dataset (as in the case of the feature denoted as d2 in Fig. 4a).

Later components (see Fig. 5b–d) account for the temporal

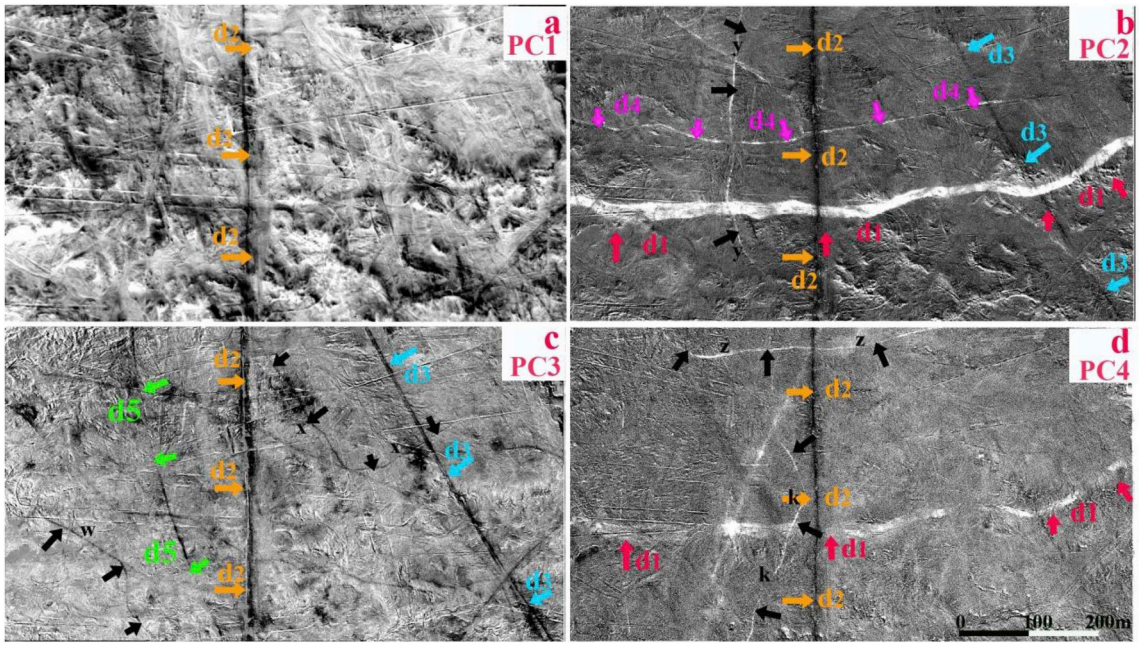

Fig. 5. The four principal components as obtained from the PCA applied to the multitemporal panchromatic satellite dataset. The arrows indicate the main disturbance features.

Table 3
Summarizes the reconnaissance of all the disturbance features from the satellite scenes and PCA components.

	Disturbance features (vehicle tracks)					Subtle disturbance features (footpaths or motorcycle tracks?)				
DATA	*d1*	*d2*	*d3*	*d4*	*d5*	*x*	*y*	*z*	*k*	*w*
2002		x	x		x					
2005		x	x		x					
2011	x	x		x						
2013	x	x								
PC1		x								
PC2	x	x	x	x			x			
PC3		x	x		x	x				x
PC4	x	x		x				x	x	

variability of the image multi-temporal dataset and well emphasize changes even small ones, as in the case of the tracks clearly highlighted in PC2, PC3 and PC4. Compared to the panchromatic scenes, some tracks are much more visible, as those indicated by purple, cyano, red and green arrows and letters d1, d3-d4 in Fig. 4b–d. As a whole, the later PCA components well evidence all the disturbance features, including the 'permanent' one (d2), due to the fact that over the years vehicles do not follow exactly the same path, causing track changes in both shape and width well revealed by the statistical de-correlation. As regards the other non-permanent disturbance features (d1, d3-d5), PC2 provides better results compared to PC3 and PC4 (see Table 3).

Ever more important is the fact that the later components put in evidence disturbances not visible from the four panchromatic images (please compare Fig. 5b–d with 4a-d). In particular, they are subtle features, probably linked to footpaths or motorcycle tracks, indicated with black arrows and letters x, y, z, k, w (see also Table 3). Moreover, we notice the 'complementarity' of PC2, PC3 and PC4 in evidencing the above said disturbance traces. In particular, the feature 'y' is only visible from PC2, 'x' and 'w' are observed only in PC3; and finally, the other two indicated with 'z' and 'k' compare only in PC4 (see Table 3).

As a whole, respect to the single panchromatic scenes (see Fig. 4) PCA provides a more complete and detailed survey of disturbance features. In particular, it evidences all the five disturbance features observed also from the panchromatic satellite dataset, plus five subtle disturbance tracks (indicated with black arrows and letters x, y, z, w, and k).

The four PC components were classified and segmented to automatically extract the changes. The results are not fully satisfactory. In particular, for each component a few disturbance tracks along with erosion are extracted. Fig. 6a shows the automatic extraction of PC2 which exhibits only three disturbance tracks and other changes linked to areas involved in erosion processes.

For this reason, further analyses have been performed using multitemporal texture analyses computed on the whole dataset such as the Standard deviation and the Skewness. The best results have been obtained from Skewness as showed in Fig. 6b–d and Table 4. In particular, we can notice that Skewness enables the visual identification of all the five 'strong' disturbance features caused by off-road vehicles (indicated with coloured arrows), and three of the five subtle one. On the eight anthropogenic disturbance recognized by visual inspection, seven are automatically extracted along with areas affected by changes probably due erosion processes.

From the rationale point of view both PCA and skewness indicators measure how much and in which direction, the values deviate from the mean. In particular, Skewness produces one image output that informs us on how much each pixel value deviate from the mean, whereas, PCA produces as output various components (whose max number is the number of the input bands), which enable us to categorize how much each pixel value deviate from the mean. Each successive component contains less of the total dataset variance and using the loadings (obtained from formula 4) PCA also provides information related to when the change occurred (namely in each input band in our case multitemporal band). From the rationale point of view, we propose the joint use of PCA and Skewness, in order to (i) immediately capture the change even subtle using the skewness (ii) maintaining from PCA the information related to how much each pixel value deviate from the mean and when this occurred. Moreover, the Skewness can enable us to automatically categorize all the changes in an easier way compared to the diverse PCA components, that can be characterized by clusters which present low internal heterogeneity and, in turn, can be more complex to automatically categorize changes using an unsupervised classification.

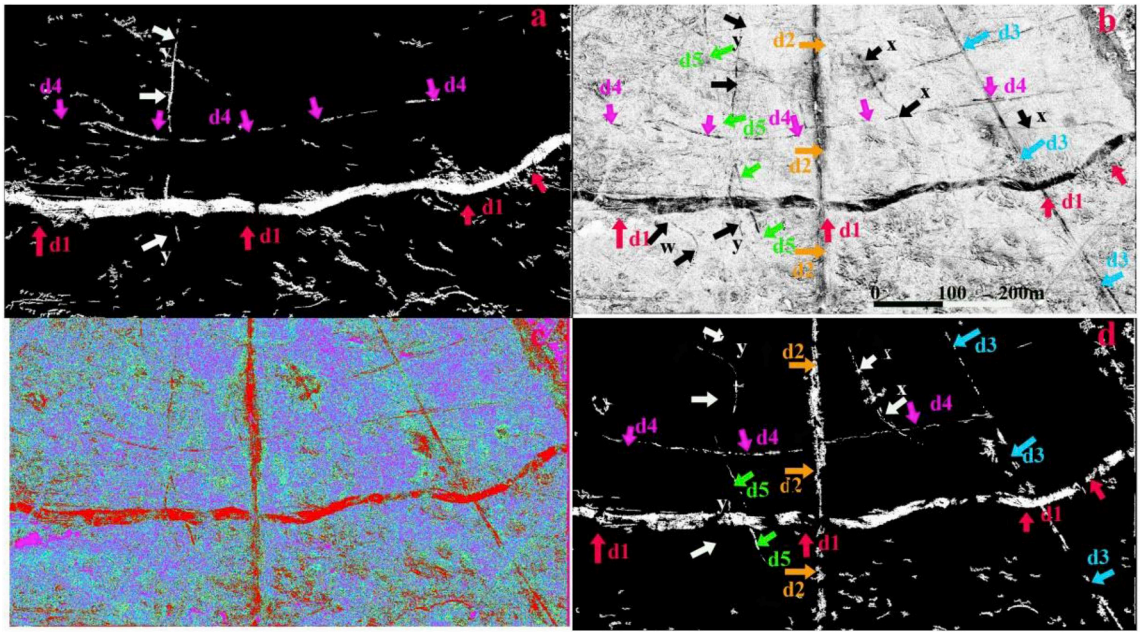

Fig. 6. (a) Automatic extraction of PC2 which exhibits three linear disturbance features, two caused by off-road vehicles and two, smaller and subtle, due to footpaths or motorcycle tracks. (b), (c) and (d) are related to Skewness, its unsupervised classification and segmentation, respectively. The Skewness allowed us to identify eight disturbance features, among the six are automatically extracted.

As a whole, we can point out that: (i) the use of both PCA and Skewness enabled us to well emphasize changes over time with particular reference to those linked to anthropogenic disturbances. PCA components provide more details, related to the number of the change features, their strength of de-correlation and the time when occurred, but, the automatic extraction is really poor being that weak categorizations are generally provided by all the PCs (except PC2). On the other side, Skewness outputs enhance a fewer number of change features compared to PCA components (eight over ten compared to) but it is suitable to automatically categorize most of changes numerically seven over eight.

For estimating the changes occurred after 2013 we re-used the correlation map computed by NASA using the L-band data acquired on 19 March 2013 and on 21 March 2015 from UAV SAR platform. To facilitate the interpretation of the correlation map we overlaid it (see Fig. 7) on the map of geoglyphs obtained as explained in section 4.2. In Fig. 7, the green colour denotes areas with higher correlation, and therefore not affected by significant changes. Whereas, yellow and orange colour characterize those areas with lower correlation values ranging from 0.5 to 0.7, thus denoting significant variations. In particular, we notice two linear patterns which follow two disturbance tracks (indicated by black arrows, and d2 and d5) already identified from the multitemporal dataset and relative outputs (PCA, textural analysis; see Figs. 4–6)). Such correlation values indicate that some changes occurred between 2013 and 2015. Consequently the disturbance activity continued after the last Dakar rally. Moreover, scattered disturbance features due probably to footpaths (pd) characterize the trapezoid and some parts of the meandering geoglyph. At northeast and southwest of the scene are indicated with letter ‘e' two areas affected by changes reasonably due to erosion processes.

As a whole, based on the results of the processing of multitemporal panchromatic dataset from 2002 to 2013 (see Figs. 4–6) and the output from the interpretation of SAR correlation map (2013 and 2015), we can conclude that respect to the ten disturbance tracks, five reasonably caused by off-road vehicles (see d1-d5 in Figs. 4–6) and 5 linked to motorcycle tracks or footpaths, only two, vehicle tracks (d2 and d5) were still in use after 2013. Local disturbance features are probably due to wind erosion and vandalism.

4.2. Enhancement and characterization of geoglyph features

In respect to the geoglyph features, considering the contribution of PCA, only the first component enabled us to enhance them. In particular, as expected, their visibility is improved by PC1 compared to the single scenes (compare Fig. 8a with Fig. 4a–d). In fact, focusing on the single scenes we notice a diverse visibility of the edges of geoglyphs, from one scene to another. For example, the trapezoid is more visible in 2002 and 2005; whereas, some of the curvilinear elements are more

Table 4
Summarizes the rate of visibility and automatic extraction of the disturbance features from PC2 and Skewness.

	Disturbance features (vehicle tracks)					Subtle disturbance features (footpaths or motorcycle tracks ?)				
DATA	d1	d2	d3	d4	d5	x	y	z	k	w
PC2-based reconaissance	x	x	x	x			x			
PC2 Autom. extract	x			x			x			
Skewness based Reconaissance	x	x	x	x	x	x	x			x
Skewness Autom. extract	x	x	x	x	x	x	x			

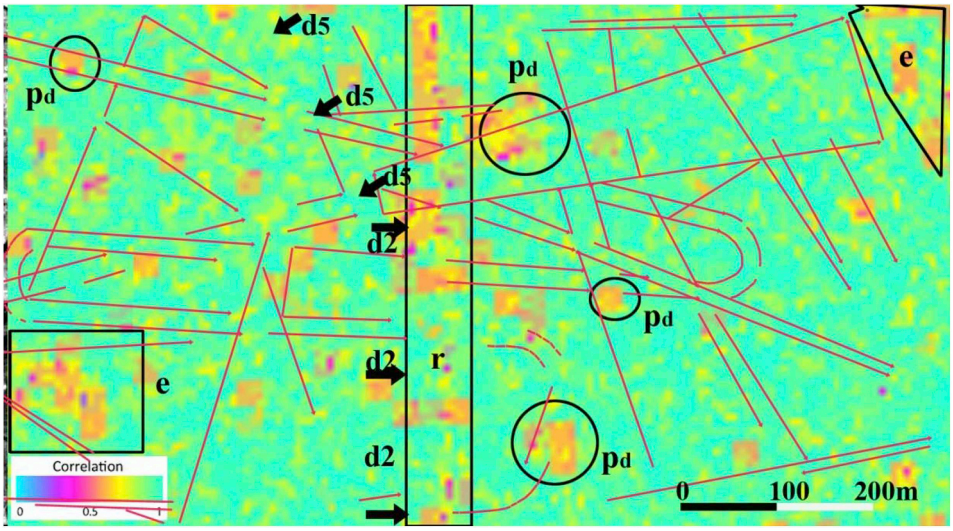

Fig. 7. UAV-SAR based correlation with geoglyphs features mapped as detailed in section 4.2. P_d denote scattered disturbance features due to footpaths, the black arrows indicate high correlation aligned along the disturbance tracks d2 and d5, as showed in Fig. 4, 'e' indicate areas affected by potential erosion processes.

visible in the 2005 and 2013 images. This is due to a number of factors such as the different sensors (see Table 1), time of acquisition, illumination conditions, noise content and disturbance of tracks. Moreover, the 2011 and 2013 images are more noisy respect to the 2002 and 2005 scenes. To reduce the noise the filtering will inevitably smooth edges of the geoglyphs, making them less visible, whereas the use of PCA minimizes the noise effect without reducing the spatial resolution. We have also to consider that the diverse wind conditions impacts on the visibility of the geoglyph edges due to the movement of desert sands. In fact, comparing the 2002 and 2005 scenes, acquired by the same sensor (QuickBird) and during the same time of the day (about 15:17 and 15.29, respectively) but, in diverse periods of the year, September and March, respectively, the visibility of the geoglyphs is different. In particular, it is better in March than in September (see Fig. 4a and b, respectively), due to the Paracas dust storms which usually affects the desert of Nasca mainly in August and in September (Briceño-Zuluaga et al., 2017). All these drawbacks are reduced exploiting the average effect of PC1, thus enhancing the geoglyph edges.

A further emphasis of the geoglyph features is obtained by using some spatial texture analyses, among which the dissimilarity provided the best results. Fig. 8 shows satellite panchromatic scene of 2005 (8a), the first component of PCA (8b), the dissimilarity computed for the 2005 (8c) and the RGB composition of dissimilarity as obtained for the single scenes acquired in 2002, 2005, and 2011 (8d). Moreover two zoomed details are showed in Fig. 8e–n. They focus the intersection of several geoglyphs. The visual comparison of the 4 scenes and zoomed details evidence the added value of dissimilarity respect to both the 2005 image and PC1 in revealing some details which helped us to understand the relative temporal sequence of geoglyphs.

Both PC1 and dissimilarities computed for the single scenes have been classified and followingly segmented in order to automatically extract geoglyph features. However, the results obtained were not satisfactory. In particular, the geoglyphs with a higher discriminability (that is with a better state of conservations) have been extracted. Whereas other subtle geoglyph features were not extracted. Finally, a huge number of false alarms make the classification useless.

On the basis of the panchromatic satellite imagery (acquired on 2002, 2005, 2011 and 2013) and derived products (PC1 and Dissimilarity), a comprehensive map of the geoglyphs has been obtained as displayed in Fig. 9a. Fig. 9b is a subset bordered by black rectangle which in Fig. 9a puts in evidence several lacunas of the geoglyphs due to disturbance tracks caused by vehicle and motorcycles, erosion processes and footpaths. These lacunas have been digitally integrated allowing us to obtain the original configuration of the geoglyphs. Such 'digital restoration' (i.e. a virtual reconstruction of geoglyphs) could be useful in the future for a real restoration of the geoglyphs, object of debate especially for the most famous biomorphic geoglyphs.

The availability of different products, in particular PC1 and dissimilarity, greatly facilitated the reconnaissance of the geoglyphs which is not an easy task, even for who had the opportunity to observe them on ground during field survey because they can be confused with other anthropic traces. In order to reduce potential errors in the reconnaissance of geoglyphs the investigation strategy also included a validation phase performed by close range surveys conducted using aircrafts and drones. These enabled a deeper analysis of geoglyphs adding details from the higher resolution DEMs and orthophotos. They were obtained by SfM-based processing of aerial and drone images (see the aerial images by aircraft and drone in Fig. 2d, e, 2f). The area surveyed by aircrafts (with spatial resolution of DEM and orthophoto equal to 31.7 cm, and 15.9 cm, respectively) was the centre of the ground drawing scene, including in particular the meandering motif (see Fig. 2ab) selected to cover this particular significant area. Whereas, the subset taken from drone (with spatial resolution of DEM and orthophoto equal to 5 cm, and 2.5 cm, respectively) was centred on an area characterized by the intersection of diverse geoglyphs (see Fig. 2ab). The DEMs have been enhanced using SVF and SLRM to emphasize edges and microtopography. In particular, SLRM well enhanced the borders of the geoglyphs because it facilitates the perception and discrimination of sunken from raised features and emphasizes height-differences between individual features and the surrounding area. SVF mainly delineated concave microrelief preserving the perception of the general microtopography.

In particular, the high detail of drone based orthophotos, DEMs and derived models were particularly useful for the spatial characterization of the intersection of geoglyphs. Fig. 10 shows a 3d detail of DEM, Orthophoto, LRM and SVF centred on the overlapping of three different geoglyphs: one trapezoid, indicated with red arrows, and two rectangular figures indicated with white and light blue arrows. The four images in Fig. 11a, b, 11c, 11d helped us in the identification of the temporal sequence (before and after) of the three geoglyphs of the subset. In particular, if we focus on the geoglyphs spatial continuity we can infer their relative temporal sequence. On the basis of this criterion, it is reasonable to assume that the trapezoid, indicated with red arrows,

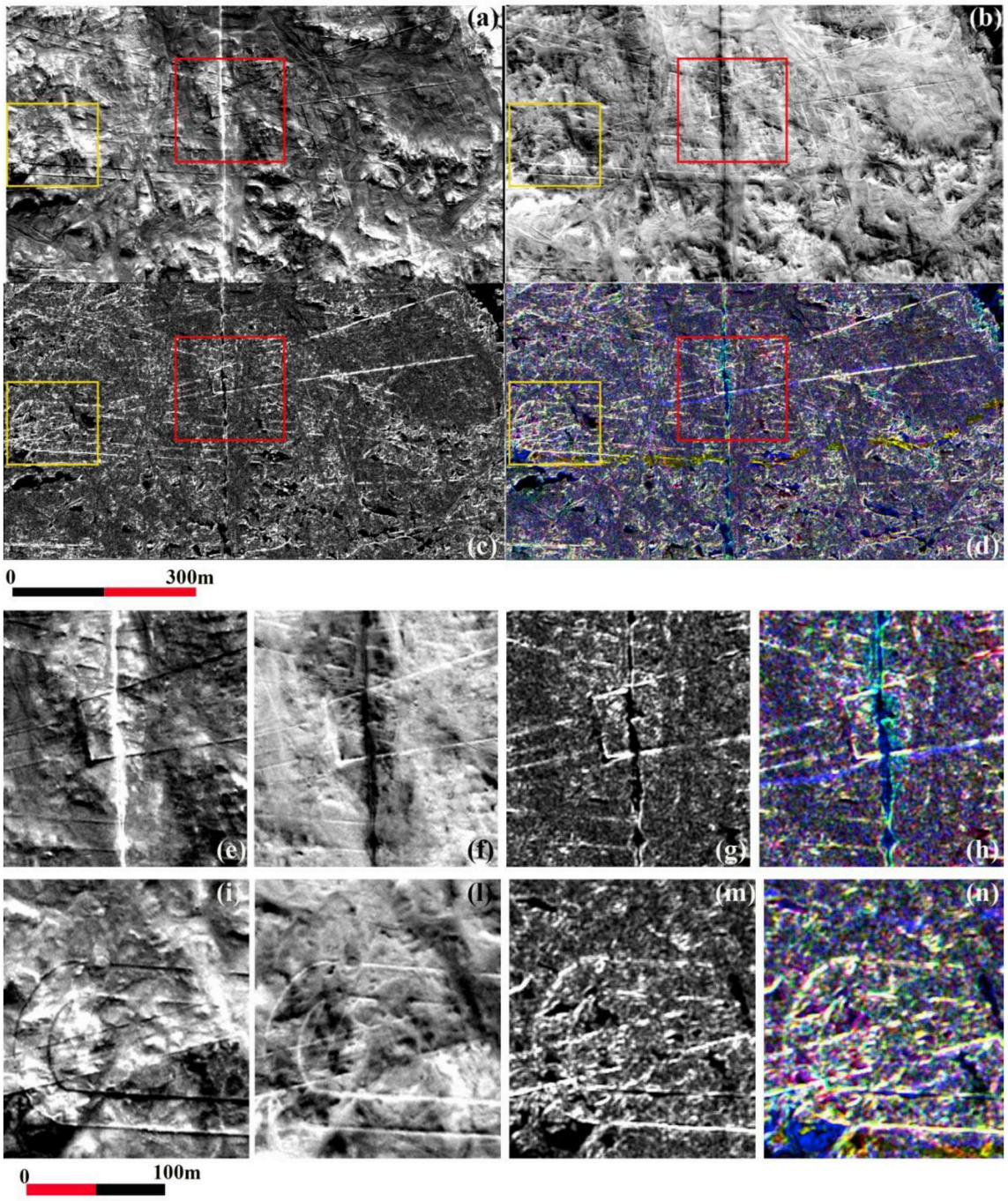

Fig. 8. (a) Satellite panchromatic scene of 2005, (b) the first component of PCA, (c) dissimilarity computed for the 2005, and (d) the RGB composition of dissimilarity as obtained for the single scenes acquired in 2002, 2005, and 2011. The two subsets (from e to n) provide the details for the two subareas related to linear and curvilinear geoglyph features in (e) to (h), and (i) to (n) respectively as in the previous figures (a–d).

has been done before the rectangular figure indicated with light blue arrows. Similarly, we can assume that the rectangular element indicated with white arrows has been done after the trapezoid. If we focus on the cross between the rectangular figures we can argue that the rectangle indicated with light blue arrows was realized after the rectangle indicated with light blue arrows. Therefore, the temporal sequence in the execution of the three geoglyphs was the following: Phase I trapezoid, phase II rectangle indicated with white arrows, phase III rectangle indicated with light blue arrows.

This approach extended to the entire scene of geoglyphs allowed us to have a comprehensive relative chronology of the area under investigation (see Fig. 11) which put in evidence four different phases of execution of the geoglyphs around the meandering figure.

As a whole, Fig. 12 shows the methodological approaches we devised for enhancing geoglyphs and for the detection and automatic extraction of disturbance features. Moreover, Fig. 12 also provides an overview of the outputs from the diverse analyses herein conducted and points out the most significant results.

5. Conclusions and future perspectives

The availability and open access to archive and novel data from

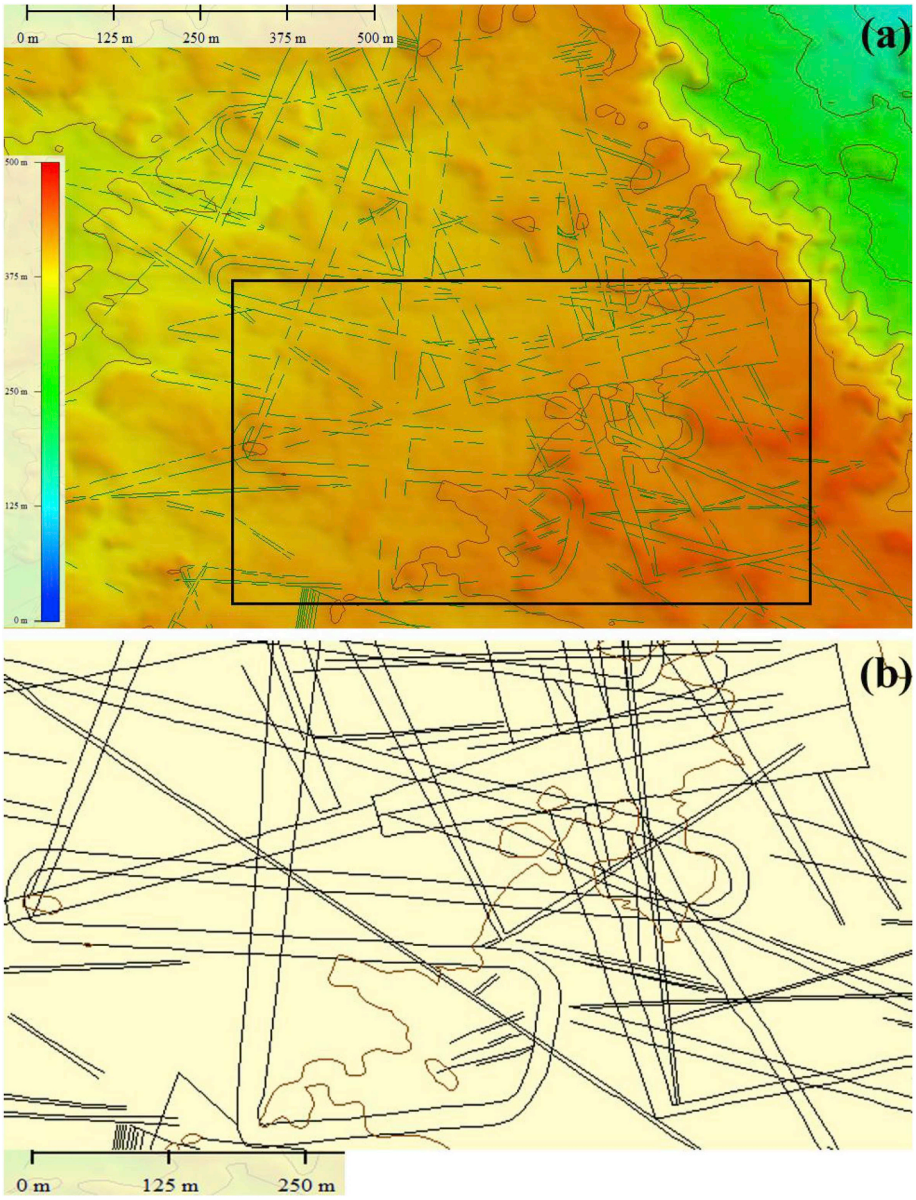

Fig. 9. (a) Map of geoglyphs. (b) 'Virtual reconstruction' of geoglyphs showed in Fig. 9a bordered by black rectangular box.

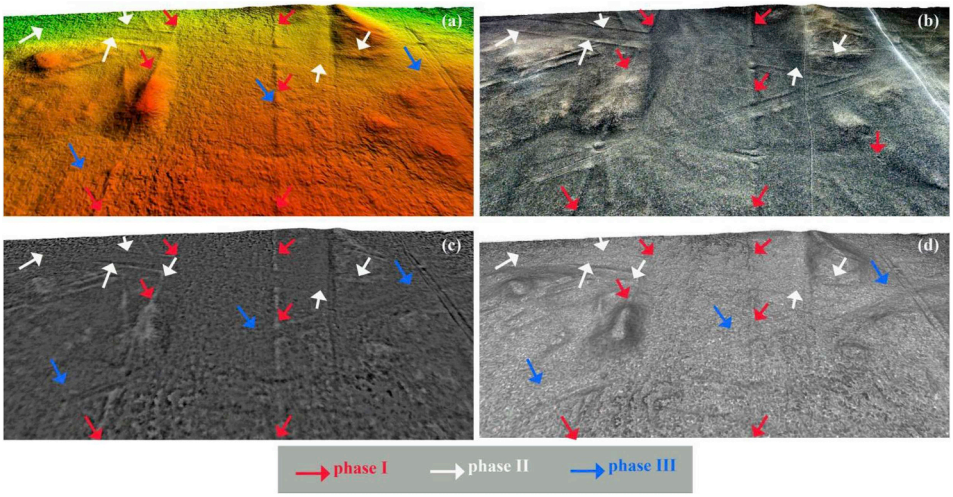

Fig. 10. 3D visualization of UAV based DEM (a), orthophoto (b), and derived texturized models obtained by computing SLRM (c) and SVF (d). The coloured arrows identify the diverse phase of drawing of the geoglyphs. The subset is located in Fig. 2d bordered by green box. (For interpretation of the references to colour in this figure legend, the reader is referred to the Web version of this article.)

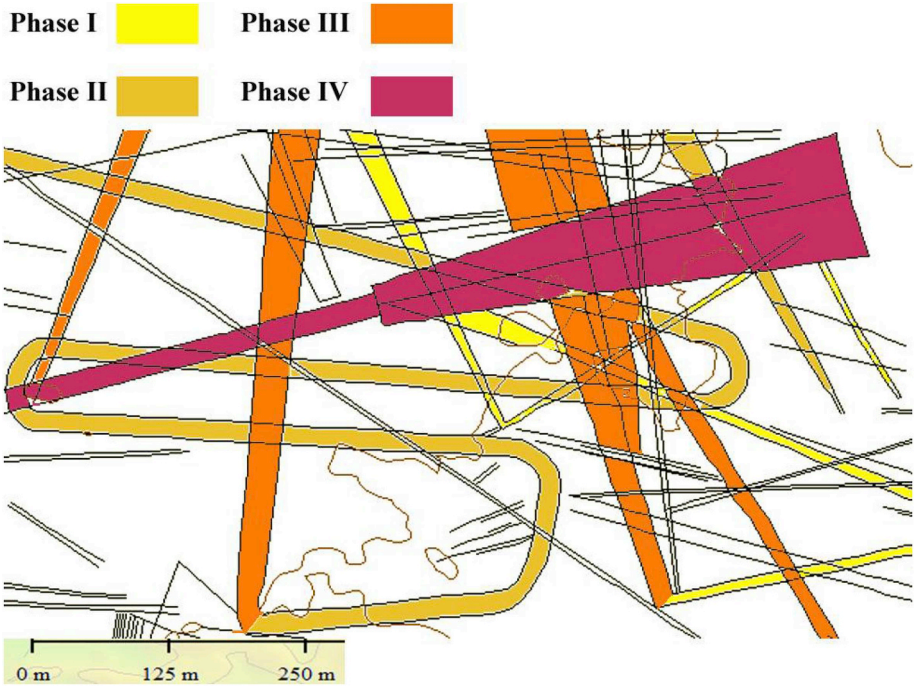

Fig. 11. Relative chronology of execution phases of geoglyphs of subset in Fig. 9b. For other geoglyphs it has not been possible to understand diachronic relation with other figures.

spaceborne and airborne platforms are today strongly increasing, thus favoring the use, reuse and integration of EO data in the cultural heritage (CH) domain, including archaeological heritage from the discovery to the monitoring, from the enhancement to the preservation. This requires efforts addressing to manage and process big data, make available reliable automatic data processing approaches and integrated methodologies of data analysis and interpretation also via case study demonstration to bridge EO technology and archaeological communities.

This paper deals with a multiscale, multisensor and multitemporal RS based approach for the analysis, interpretation and monitoring of Nasca geoglyphs which are one of the most impressive and vulnerable examples of cultural heritage throughout the entire world. They are exposed to damage much more than any other cultural heritage, due to their intrinsic fragility but also because they are characterized by very subtle features and strongly threatened by several anthropogenic factors.

The area investigated in this paper is located in Pampa de Atarco, selected because it is representative of the most fragile geoglyphs, much more than those already investigated in other sites, such as Pampa de Nasca (Hesse, 2015; Comer, 2017) and Palpa (Lambers, 2006). This is due to the specific engraving techniques based on the use of sand grain, pebbles and gravel of small dimension which make the geoglyphs very difficult to be detected not only on ground but also by satellite and close range view, especially in not optimal illumination condition. This has suggested an investigation strategy based on the integration of multiscale remote sensing passive and active data, including close range imagery, to enhance the visibility of geoglyphs (most of them are very subtle) and to capture the changes due to human induced disturbance affecting them. To cope with these issues, the analyses herein performed were based on statistical indicators computed in both temporal and spatial domain. Multitemporal analysis of VHR satellite imagery using PCA and Skewness allowed us to enhance the visibility of disturbance features and to automatically extract them using unsupervised classifications. In particular, respect to the satellite multitemporal data set which reveals the presence of five off-road vehicle tracks, the enhancement by PCA and Skewness enabled to add other five thinner tracks referable to footpaths or motorcycle tracks. The best results in terms of enhancement and automatic extraction capability of disturbance features have been obtained by Skewness.

The reuse of UAV L SAR-based correlation map, available free of charge from NASA, provided useful information on the state of disturbance from 2013 to 2015, widening the observation time window of the VHR satellite data set from 2002 to 2013.

In the spatial domain, the textural analyses mainly based on dissimilarity along with PC1 enabled us to enhance edges of geoglyphs features facilitating their mapping and interpretation. In particular, in areas characterized by the superposition of geoglyphs, thanks also to the contribution of close range UAV photogrammetry, it was possible to reconstruct the relative chronological sequence thus providing an important contribution to archaeological studies. In the future, it is desirable to improve the relative chronological method with approaches and tools for absolute dating. This can be achieved by the analysis of pottery and ceramics close and along the geoglyphs, previously identified using Remote sensing data.

As a whole, results from our investigations pointed out that the integration of satellite-based imaging and information with manned and unmanned data have significant potential to contribute into decision making processes for improving knowledge and supporting systematic monitoring and sustainable management strategies as mandatory steps to preserve unique or un-renewable resources as cultural heritage and landscape.

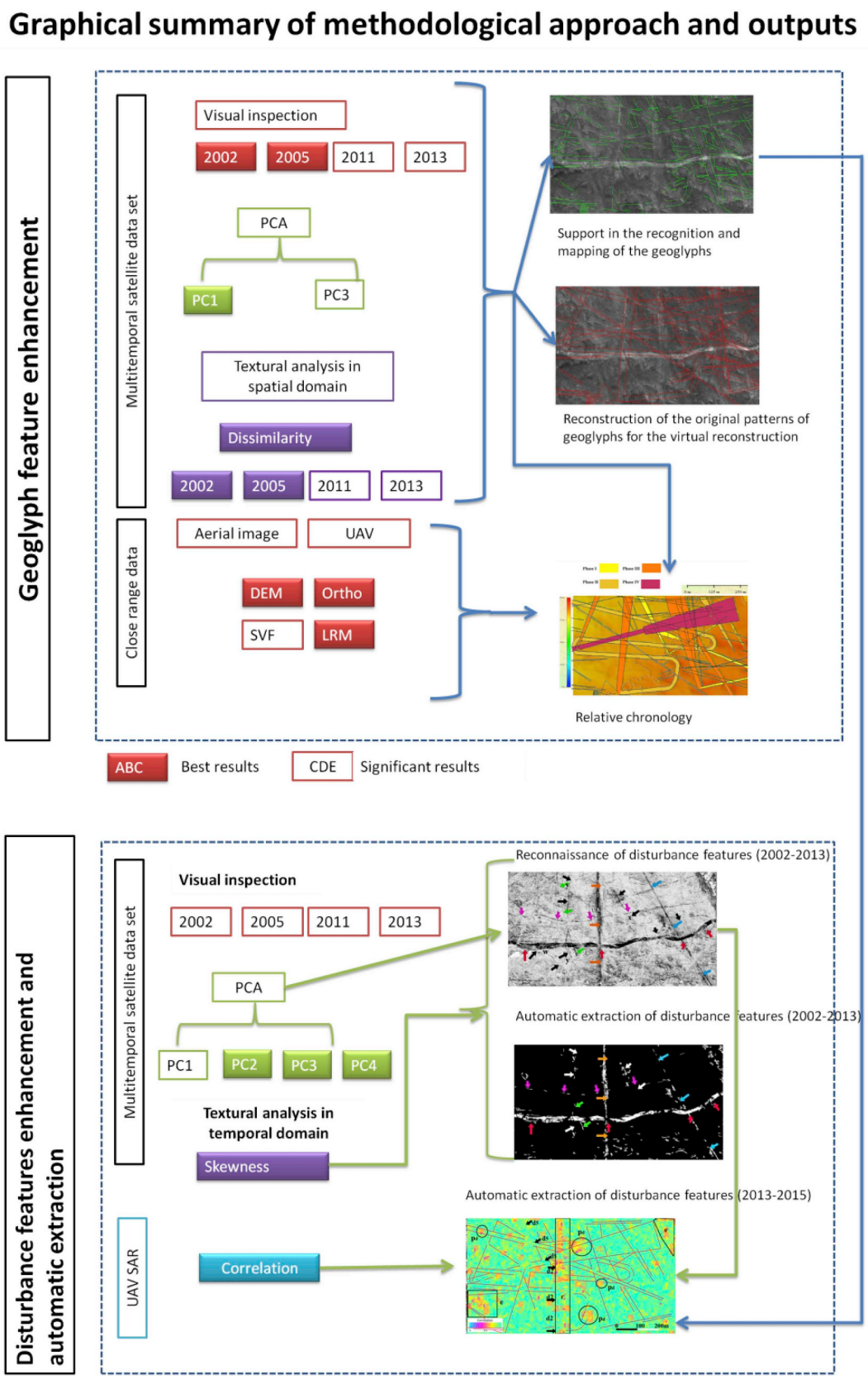

Fig. 12. Graphic summary of the two multiscale, multisensor and multitemporal approaches: one devised for enhancing geoglyphs, the second for detecting and automatically extracting disturbance features.

Acknowledgement

The investigations have been funded by Joint Laboratory of Prehispanic Archaeological Science (LaPAS) funded by CNR. We thank Giuseppe Orefici for his support in archaeological interpretation, Manuela Scavone for digital mapping of geoglyphs, Antonio Pecci for drone surveys, Maria Danese for GIS based analyses, Maria Sileo for her contribution to field surveys.

APPENDIX

Principal Component Analysis

The PCA is based on the covariance (or variance) matrix (S) computed among all input time series, the eigenvalues, eigenvectors and loadings using formulas 1a-4

$$\mathrm{covk_1k_2} = \frac{1}{n \times m}\sum_{i=1}^{n}\sum_{j=1}^{m}\left(SB_{i,j,k_1} - \mu_{k_2}\right) \times \left(SB_{i,j,k_2} - \mu_{k_2}\right) \quad [1a]$$

where k_1, k_2 are two input spectral channels, $SB_{i,j}$ is the spectral value of the given channel in row *i* and column *j*, *n* number of row, *m* number of columns, μ is the mean of all pixel $SB_{i,j}$ values in k_1 and k_2

The most common application of PCA is based on the use of covariance matrix, even if both variance and covariance measure the "spread" of a dataset around the mean. A series of new image layers (eigenvectors generally called eigenchannels or components) are obtained from the eigenvalues of the covariance matrix (using formula 2 and 3). The percentage of total dataset variance, explained by each component, is obtained by formula 2:

$$\%\,i = 100 \times \vartheta_i / \sum_{i=1}^{k}\lambda_i \quad [2]$$

where $\%\, i_i$ are eigenvalues of S.

Finally, a series of new image layers (called eigenchannels or components) are computed (formula 3) by multiplying, for each pixel, the eigenvector of S for the original value of a given pixel in the input bands

$$P_i = \sum_{i=1}^{n} P_k \times u_{k,i} \quad [3]$$

where P_i indicates a spectral channel in component i, $u_{k,i}$ eigenvector element for component i in input band k, P_k spectral value for channel *k*, number of input band.

A loading, or correlation R, of each component i with each input date k can be calculated by using formula 4.

$$R_{k,i} = u_{k,i} \times (\lambda_i)^{\frac{1}{2}} \times (var_k)^{1/2} \quad [4]$$

where var_k is the variance of input date *k* (obtained by reading the *k*th diagonal of the covariance matrix.

Skewness measurement

The most common skewness measurement is Fisher-Pearson (or Pearson median skewness) expressed by formula 5

$$\mathrm{Skewness} = \frac{1}{N}\sum_{J=1}^{N}\left(\frac{x_j - \bar{xi}}{\text{Standard deviation}}\right)^3 \quad [5]$$

where x_j is the value of the pixel for band j, N is the number of the images, in our case satellite scenes acquired in a different time, $\bar{xi}$ is the mean

$$\text{Standard deviation} = (\text{variance})^{1/2}$$

$$\mathrm{Variance} = \frac{1}{N-1}\sum_{J=1}^{N}(x_j - \bar{xi})^2 \quad [6]$$

Texture Indicators

The Variance that measures local variance of the processing window

$$\mathrm{Variance} = \sum_i \sum_j (i-u)^2 (pi, j) \quad [7]$$

- The Correlation that measures the linear dependency of a gray level on those of neighbouring image cells.

$$\mathrm{Correlation} = \frac{\sum_i \sum_j \boldsymbol{p(i,j)} - \boldsymbol{m\,x\,m\,y}}{\boldsymbol{s\,x\,s\,y}} \quad [8]$$

- Contrast that measures gray-level contrast by using weighting factors equal to the square of the gray level difference.

$$\text{Contrast} = \sum_{n=0}^{Ng-1} (n)^2 \sum_{i=1}^{Ng} \sum_{j=1}^{Ng} p(i,j) \quad [9]$$

- Dissimilarity that uses weighting factors equal to the absolute value of the gray level difference, so

$$\text{Dissimilarity} = \sum_{n=0}^{Ng-1} (n) \sum_{i=1}^{Ng} \sum_{j=1}^{Ng} p(i,j)^2 \quad [10]$$

- Homogeneity measures the smoothness of the image area.

$$\text{Homogeneity} = \sum_i \sum_j \frac{1}{1+(i-j)^2} p(i,j) \quad [11]$$

- Entropy that measures the randomness or disorder of the image area.

$$\text{Entropy} = \sum_i \sum_{j=1} p(i,j) \log(pij)) \quad [12]$$

Where, in equations 7 to 12, i, j are coordinates of the co-occurrence matrix space; p (i, j) is the element of the i and j coordinates; and Ng is dimension of the co-occurrence matrix, which has gray value range of the original image. Finally, in equation (8) m and s denote average and standard deviation, respectively.

References

https://uavsar.jpl.nasa.gov/cgi-bin/data.pl.

https://whc.unesco.org/en/list/700.

UNESCO, 1994. Convention concerning the protection of the world cultural and natural heritage, world heritage committee, eighteenth session phuket. Thailand 12–17 December 1994.

Alva, W., Meneses Alva, S., 1984. Geoglifos del Formativo en el valle de Saña. Lundero. Suplemento cultural del diario La Industria. Chiclayo, 24 de Junio.

Aveni, A.F., 1986. The Nasca lines: patterns in the desert. Archaeology 39 (4), 32–311.

Balakrishnan, N., Scarpa, B., 2012. Multivariate measures of skewness for the skewnormal distribution. J. Multivar. Anal. 104, 73–87.

Ball, G.H., Hall, D.J., 1965. ISODATA, a Novel Method of Data Analysis and Pattern Classification. Stanford Research Institute, Menlo Park.

Briceño-Zuluaga, F., Castagna, A., Rutllante, J.A., et al., 2017. Paracas dust storms: sources, trajectories and associated meteorological conditions. Atmos. Environ. 165, 99–110.

Briones, M.L., 2006. The geoglyphs of the north Chilean desert: an archaeological and artistic perspective. Antiquity 80, 9–24.

Casu, F., Manunta, M., Agram, P.S., Crippen, R.E., 2017. Big remotely sensed data: tools, applications and experiences. Remote Sens. Environ. 202 (1), 1–2.

Chapman, B., Comer, D., Isla, J.A., Silverman, H., 2015. The measurement by airborne synthetic aperture radar (SAR) of disturbance within the Nasca world heritage site. Conserv. Manag. Archaeol. Sites 17, 270–286 2015.

Chen, F., Masini, N., Liu, Jie, You, Jiangbin, Lasaponara, R., 2016. Multi-frequency satellite radar imaging of cultural heritage: the case studies of the Yumen Frontier Pass and Niya ruins in the Western Regions of the Silk Road Corridor. Int. J. Digit. Earth 9 (12), 1224–1241. https://doi.org/10.1080/17538947.2016.1181213.

Cigna, F., Tapete, D., 2018. Tracking human-induced landscape disturbance at the Nasca lines UNESCO world heritage site in Peru with COSMO-SkyMed InSAR. Remote Sens. 10, 572.

Comer, D.C., Chapman, B.D., Comer, J.A., 2017. Detecting landscape disturbance at the Nasca lines using SAR data collected from airborne and satellite platforms. Geosciences 7, 106.

Delle Rose, M., 2016. The geology of Cahuachi. In: Lasaponara, R., Masini, N., Orefici (Eds.), Ancient Nasca World. New Insights from Science and Archaeology. Springer, pp. 47–64.

Eitel, B., Hecht, S., Mächtle, B., Schukraft, G., et al., 2005. Geoarchaeological evidence from desert loess in the Nasca-Palpa region, southern Peru: palaeoenvironmental changes and their impact on Pre-Columbian cultures. Archaeometry 47 (1), 137–158.

Erickson, C.L., 2010. The transformation of environment into landscape: the historical ecology of monumental earthwork construction in the Bolivian Amazon. Diversity 2, 618–652.

Hesse, R., 2010. LiDAR-derived Local Relief Models a new tool for archaeological prospection. Archaeol. Prospect. 17, 67–72.

Hesse, R., 2015. Combining Structure-from-Motion with high and intermediate resolution satellite images to document threats to archaeological heritage in arid environments. J. Cult. Herit. 16, 192–201.

Irons, J.R., Petersen, G.W., 1981. Texture transforms of remote sensing data. Remote Sens. Environ. 11, 259–370.

Kosok, P., Reiche, M., 1949. Ancient drawings on the desert of Peru. Archaeology 2 (4), 206–215 19411.

Kozak, R., 15 Dec 2014. The wall street journal. Peru says greenpeace permanently damaged nazca lines. Available online: https://www.wsj.com/articles/peru-says-greenpeace-permanently-damaged-nazca-lines-1418681478, Accessed date: 8 May 2019.

Lambers, K., 2006. The Geoglyphs of Palpa (Peru): Documentation, Analysis, and Interpretation., Aichwald : Linden Soft. vol. 2 Series Forschungen zur Archäologie außereuropäischer Kulturen.

Lasaponara, R., Masini, N., 2017. Preserving the past from space: an overview of risk estimation and monitoring tools. In: Masini, N., Soldovieri, F. (Eds.), Sensing the Past. From Artifact to Historical Site. Springer International Publishing, pp. 61–88. https://doi.org/10.1007/978-3-319-50518-3_3.

Lasaponara, R., Masini, N. (Eds.), 2008. Advances in Remote Sensing for Archaeology and Cultural Heritage Management, Proc. Of I International EARSeL Workshop "Advances in Remote Sensing for Archaeology and Culturale Heritage Management", Rome 30 Septembre-4 October, 2008. 978-88-548-2030-2, Aracne, Roma, 2008.

Luo, L., Wang, X., Guo, H., Lasaponara, R., Zong, X., Masini, N., Wang, G., Shi, P., Katteli, H., Chen, F., et al., 2019. Airborne and spaceborne remote sensing for archaeological and cultural heritage applications: a review of the century (1907–2017). Remote Sens. Environ. 232, 111280. https://doi.org/10.1016/j.rse.2019.111280.

Masini, N., Orefici, G., Danese, M., Pecci, A., Scavone, M., Lasaponara, R., 2016a. Cahuachi and Pampa de Atarco: towards greater comprehension of Nasca geoglyphs. In: Lasaponara, R., Masini, N., Orefici, G. (Eds.), The Ancient Nasca World New Insights from Science and Archaeology. Springer International Publishing, pp. 239–278. https://doi.org/10.1007/978-3-319-47052-8_12. 2016.

Masini, N., Danese, M., Pecci, A., Scavone, M., Lasaponara, R., 2016b. Nasca lines: space tracking of vandalism. In: Lasaponara, R., Masini, N., Orefici, G. (Eds.), The Ancient Nasca World New Insights from Science and Archaeology. Springer International Publishing, pp. 635–656. https://doi.org/10.1007/978-3-319-47052-8_26. 2016.

Masini, N., Orefici, G., Lancho Rojas, J., 2016. Nasca geoglyphs: technical aspects and overview of studies and interpretations. In: Lasaponara, R., Masini, N., Orefici, G. (Eds.), The Ancient Nasca World New Insights from Science and Archaeology. Springer International Publishing, pp. 217–238 2016.

Neeti, N., Eastman, J.R., 2014. Novel approaches in Extended Principal Component Analysis to compare spatio-temporal patterns among multiple image time series. Remote Sens. Environ. 148, 84–96.

Opitz, R., Herrmann, J., 2018. Recent trends and long-standing problems in archaeological remote sensing. Journal of Computer Applications in Archaeology 1 (1), 19–41.

Orefici, G., 2009. Los geoglifos: espacios abiertos y ceremonias colectivas. In: Nasca. El desierto de los Dioses de Cahuachi. Graph Ediciones, Lima, pp. 94–113.

Orefici, G., Lancho Rojas, J., 2016. The Nasca area and its environment. In: Lasaponara, R., Masini, N., Orefici (Eds.), Ancient Nasca World. New Insights from Science and Archaeology. Springer, pp. 21–45.

Reindel, M., Wagner, G.A., 2009. New Technologies for Archaeology: Multidisciplinary Investigations in Nasca and Palpa, Peru. Springer, Heidelberg, Berlin.

Reinhard, J., 1988. The nazca lines, water and mountains: an ethno-archaeological study. In: Saunders, N., de Montmollin, O. (Eds.), Recent Studies in Pre-columbian Archaeology. British Archaeological Reports, Oxford, pp. 363–414.

Richards, J.A., Jia, X., 2006. fourth ed. Remote Sensing Digital Image Analysis –

Hardback Springer, 1148 Berlin/Hiedelberg, pp. 476.
Roselló, L., Huaypa, M.C., Mazzotti, P.L., 1985. Rayas y Figuras en la Pampa Canto Grande. Revista del Museo 39, 41–58.
Ruescas, A., Delgado, J., Costantini, F., Sarti, F., 2010. Change Detection by Interferometric Coherence in Nasca Lines, Peru (1997–2004). In: Proceedings of the Fringe 2009 Workshop, Frascati, Italy, 30 November 2009–4 December 2009.
Saunaluoma, S., Schaan, D., 2012. Monumentality in Western Amazonian formative societies: geometric ditched enclosures in the Brazilian state of Acre. Antiqua 2, e1. https://doi.org/10.4081/antiqua.2012.e1.
Schreiber, K.H., Lancho Rojas, J., 2009. El control del agua y los puquios de Nasca. In: Nasca. El desierto del los Dioses de Cahuachi, Graph, Lima, pp. 132–151.
Silverman, H., 1990. Beyond the Pampa: the geoglyphs in the valley of nazca. Natl. Geogr. Res. 6 (4), 435–456 (Washington D. C).
Zakšek, K., Oštir, K., Kokalj, Ž., 2011. Sky-view factor as a relief visualization technique. Remote Sens. 3, 398–415.